IEEE Journal of Microwaves

Received 5 October 2022; revised 1 December 2022; accepted 2 December 2022. Date of publication 19 December 2022; date of current version 6 January 2023.

Digital Object Identifier 10.1109/JMW.2022.3226884

Motion-Modulated Chipless RFID

ASHKAN AZARFAR (Graduate Student Member, IEEE), NICOLAS BARBOT (Member, IEEE), AND ETIENNE PERRET (Senior Member, IEEE)

(Invited Paper)

University of Grenoble Alpes, Grenoble INP, LCIS, F-26000 Valence, France

CORRESPONDING AUTHOR: Ashkan Azarfar (email: ashkan.azarfar@lcis.grenoble-inp.fr).

This work was supported by the European Research Council (ERC) through the European Union's Horizon 2020 Research and Innovation Program (ScattererID) under Grant 772539.

This work did not involve human subjects or animals in its research.

ABSTRACT This paper addresses the new type of backscatter communication based on motion-modulated chipless Radio Frequency IDentification (RFID) tags. To clearly explain the concept, the different methods of backscatter communication are classified from a system point of view based on the two fundamental properties of linearity and variation in time. The principle of classical chipless RFID technology, as a non-modulated backscatter method, and the motion-modulated chipless RFID are described with general mathematical demonstrations, while the performance of the two approaches is compared in terms of read range. Motion-modulated chipless RFID is presented as an effective backscatter communication method for identification and sensing of moving objects at large distances. Three different types of motion-induced modulation as phase (Doppler) modulation, polarization modulation, and directional modulation are addressed based on three specially designed moving resonant scatterers. The modulation process in each case is theoretically described, and the performance of the motion-modulated tag is experimentally verified in terms of identification capability and large read range.

INDEX TERMS Backscatter communication, chipless RFID, doppler, motion-modulated chipless RFID, MTT 70th Anniversary Special Issue.

I. INTRODUCTION

Backscatter communication methods, as it is illustrated in Fig. 1, can be classified into two main categories as modulated backscatter and non-modulated backscatter techniques in which the functionality of the transponder can be respectively modeled as a time-variant (TV) and a time-invariant (TI) system. Then, the both categories are classified based on linearity, which results in four general classes for backscatter communication with non-linear time-variant (NLTV), linear time-variant (LTV), linear time-invariant (LTI), and non-linear time-invariant (NLTI) transponder. Since this paper is focused on linear techniques, the non-linear methods, NLTV and NLTI, are only mentioned by [1] and [2] respectively to provide a general view, and so they have been shown in gray color in Fig. 1. For both LTV and LTI transponders, the magnitude of the reflected electromagnetic (EM) wave is linearly proportional to the magnitude of the incident EM wave. However, the main difference between the two linear techniques (LTV and LTI) is that the backscattered EM wave from an LTV transponder is modified during the time while the backscattered wave from an LTI transponder remains invariant over time. Basically, an energy source as a modulation source should be provided in an LTV transponder such that its properties is modified relative to the data during the time. As it is shown in Fig. 1, this modulation source is either electrical or mechanical which can be supplied by the transponder itself (active LTV transponder) or be captured by the transponder from external sources available in the environment (passive LTV transponder). With this proposed general classification in mind, we explore historically all the linear backscatter communication methods presented up to now, while all of them can be fitted in this categorization. Moreover, this classification is used to accurately address the presented work among all the other types of backscatter communications.

The earliest backscatter communication system was invented in 1880 when Alexander Graham Bell realized an optical backscatter communication link called photophone [3]. In a photophone, the sound waves (human

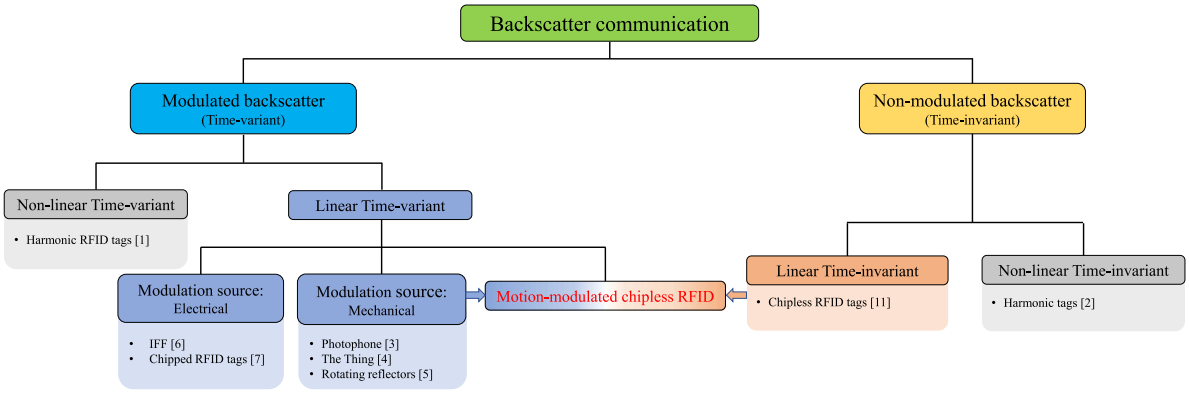

FIGURE 1. **Classification of backscatter communication methods.**

speech) incident on a flexible mirror caused to vibrate its reflecting surface and produce a modulation on the reflected light beam which carries the speech signal. According to the best knowledge of the authors, the photophone is the first realized example for LTV backscattering transponder. With a similar idea but in Radio Frequency (RF) band, a spy listening LTV transponder called "The Thing" was developed by Leon Theremin in 1945 [4]. The device was basically a cavity-loaded antenna in which the impedance seen by the antenna was modulated with sound waves impinging on the flexible membrane of the resonant cavity, and consequently, the backscattered RF waves from the antenna carried the speech of those close to the device. Afterward, in 1948, Harry Stockman in his landmark paper [5] classified the different types of linear backscatter modulation (modulation done by LTV transponders) as "variable-damping modulation", "phase (Doppler) modulation", "directional modulation", and "polarization modulation". In other words, Stockman has demonstrated that a "modulated reflector" (or an LTV transponder) can be realized based on any phenomenon which changes the scattering properties of the reflector (scatterer) so that, the backscattered wave is modified in magnitude, phase, or polarization during the time. Stockman has explored the concept comprehensively in theory, and he addressed practical examples for mechanically modulating LTV transponders realized based on rotating corner reflectors. It should be mentioned that the mechanical modulation source in [3] and [4] (vibration) was captured from the sound waves (passive LTV transponder), while in [5] the rotational motion was applied to the corner reflectors using electric motors (active LTV transponder). In addition, the modulation data in all these cases [3], [4], [5] was directly associated with mechanical sources, which are speech data carried by the sound waves in [3] and [4], and the rotational speed in [5].

Although the modulation source in most of the early backscatter communications was mechanical, the use of electronic switching elements got widely attracted in afterward years as an effective method for backscatter modulation with electrical source. This technique started from 1940 when the earliest Identification Friend or Foe (IFF) system was developed using switches which make the dipole scatterers mounted on the aircraft short or open circuited, and consequently modulate the radar echo of the aircraft like an active LTV transponder [6]. This was the beginning of the development path for chipped RFID technology which today is used extensively in everyday life and in commercial applications [7]. The chipped RFID tags basically consist of an antenna loaded by the electronic switching chip which modulates the backscattering from the antenna [8]. The electrical energy required for the modulation in chipped RFID tags can be supplied by the built-in batteries in semi-passive chipped RFID tags (active LTV transponder) or can be harvested from the incident EM waves in passive chipped RFID tags (passive LTV transponder) [7], [9]. Obviously, the modulation data in the chipped RFID technology is also associated with (or stored in) the electronic chip. The great advancement of electronics in recent decades has paved the way to implement more efficient and less-cost electronic chips for chipped RFID tags, however, the fabrication cost for chipped tags is still quite large compared to the optical barcodes which are used in massive identification processes. In addition to the cost issue, chipped RFID tags has a much more complex implementation compared to barcodes. Furthermore, the large-scale use of silicon chips has a strong impact in terms of environmental pollution. As an intermediate solution between chipped RFID tags and barcodes, chipless RFID technology has been recently introduced to significantly lower the tag fabrication cost by removing the electronic chip from the tag structure, and to relatively alleviate the complexity and environmental issues [10], [11], [12]. In this technique, the identification data are included in the physical and geometrical properties of the chipless tags which are made from passive linear materials (conductors and dielectrics), and the structural encoded data in the tags is translated to their frequency or time domain backscattering response (frequency-coded tags based on multiple resonant scatterers and time-coded tags based on multiple reflectors along a transmission line) [11]. Thus, as there is no time-varying property involved in this technique, chipless tags can be considered as LTI transponders which will be discussed in Section II. Although the chipless

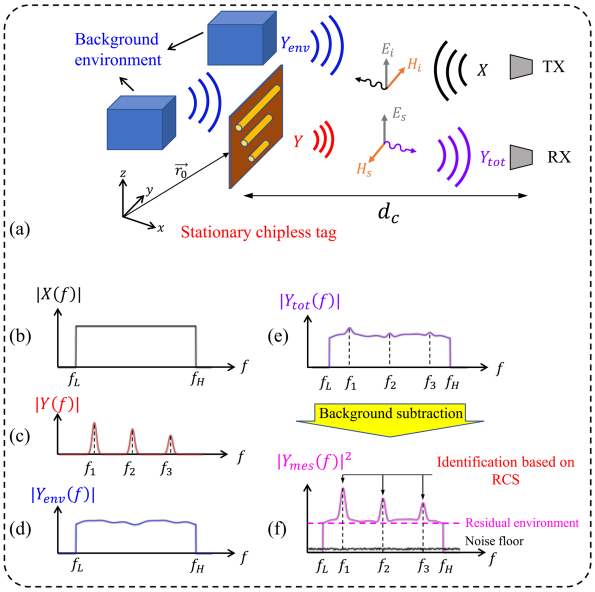

FIGURE 2. (a) Classical communication scenario to identify stationary frequency-coded chipless tags in a real environment. (b) Interrogating signal. (c) Tag response. (d) Environment response. (e) Total received response. (f) PSD of the measured tag response.

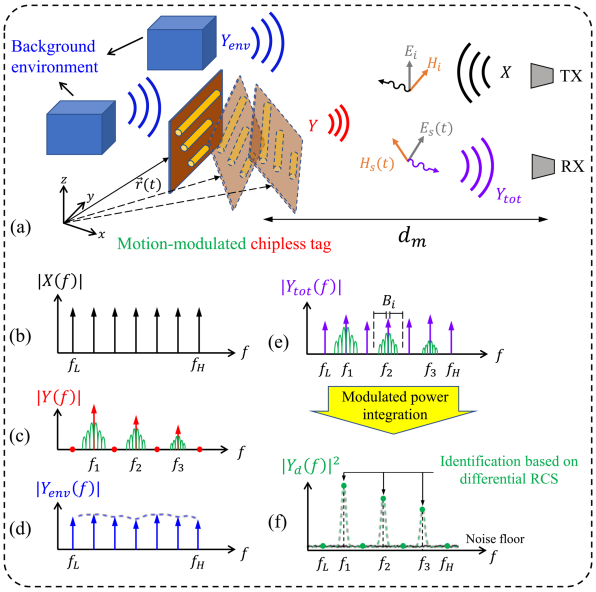

FIGURE 3. (a) Proposed communication process to identify a motion-modulated chipless tag. (b) Interrogating signal. (c) Tag response. (d) Environment response. (e) Total received response. (f) PSD of the differential backscatter power.

approach provides more desirable tags (less expensive, less complex, and more environmentally compatible) compared to chipped RFID, the chipless technology faces some challenges in terms of the coding capacity, reading distance, and reader complexity [11]. During the last decade, the chipless RFID has been developed and widely considered by research groups to introduce efficient coding approaches [13], [14], [15], [16], robust detection methods [17], [18], [19], [20], and novel designs for reader architecture [21], [22], [23]. Nevertheless, compared to the above subjects, fewer studies have focused on the read range limitation of the chipless tags and the possible ways to increase the reading distance [24], [25]. In fact, the achieved read range for chipless tags in most studies is limited by 1 m which is much lower than what can be reached for chipped UHF RFID tags.

The study conducted in [26] has demonstrated that the chipless read range is fundamentally limited due to the inherent property of the chipless tags which behave as an LTI transponder. This fact is addressed well in Section II. Indeed, in a real environment where almost all the objects are stationary and behave as LTI systems (as same as chipless tags), contribution of the tag can not be easily separated form the ones due to the environment, which limits the read range of the chipless tags. Obviously, the only effective solution for breaking this read range limitation is to violate the LTI property for chipless tags.

Coming back to the early backscatter modulation techniques, motion (as a time-varying phenomenon) can be used to modulate the scattering from chipless tags and to realize LTV transponders which can be detected at larger distances. As it is illustrated in Fig. 1, this type of LTV transponders that are called in the following "motion-modulated chipless tags" have some shared properties between the mechanical LTV transponders and the chipless tags as LTI transponders. In other words, the identification data for motion-modulated chipless tags are associated with the structural properties of the tags (and not linked with the motion properties like what was presented in [3], [4], [5]), while the motion effect is just utilized to modulate the backscattered wave such that the data encoded into the structural properties of the chipless tag can be retrieved from the motion-modulated wave. For this reason, the same chipless RFID tag can belong to both the "Motion-modulated chipess RFID" and "Linear Time-invariant" categories. Since Stockman work, only few papers have investigated motion-modulated chipless tags. One remarkable example is addressed in [27] where a rotating chipless tag was read at a distance of 2 m. It should be mentioned that, for a time-harmonic incident wave, a moving scatterer (reflector) can modulate the backscattered wave during the time in terms of different physical parameters (magnitude, phase, and polarization), while all of them are translated to an amplitude modulation, a phase modulation, or a mixed amplitude-phase modulation on the received signal.

This paper reviews different types of motion-modulated chipless tags which have been recently developed by the authors. The performance of the motion-modulated chipless RFID has been demonstrated theoretically and proved experimentally for all the types. The authors expect that this approach will open promising prospects for chipless RFID to identify and to sense moving objects in real scenarios at large distances.

The paper is organized as follows. Section II presents the general advantages of the motion modulated chipless RFID compared to classical chipless RFID in terms of reader architecture, detection robustness, and read range. The

phase (Doppler)-modulated chipless tags, the polarization-modulated chipless tags, and the direction-modulated chipless tags are respectively demonstrated in Sections III, IV, and V. Finally, Section VI concludes the paper.

II. CHIPLESS RFID VS. MOTION-MODULATED CHIPLESS RFID

A. CHIPLESS TECHNOLOGY: LTI TRANSPONDER BASED ON RCS

1) PRINCIPLE

Fig. 2 presents the backscattering from a frequency-coded chipless tag and the classical reading process in frequency domain chipless technology. The example tag consists of three different-length dipole scatterers (realized on a dielectric substrate) resonating at three different frequencies as f_1, f_2, and f_3. Most of the time chipless tags consist of resonant scatterers and are modeled as simple RLC circuits. Values of R, L, or C are linked to the structural parameters (dimensions, spacing, or any other physical parameters) of the tag [11]. However, the most important physical property behind all the presented models is that the chipless tag can be considered as an LTI system. In fact, since all the components of the tag are electromagnetically linear and there is no time-variation aspect in the tag structure [of course when it is supposed to be stationary in space, e.g. at r_0 in Fig. 2(a)], the LTI model can accurately describe the chipless tag with a very general view. In order to interrogate the tag, classically, a UWB signal $X(f)$ in the form of an EM plane wave is sent toward the tag, which is ideally shown in Fig. 2(b) with a constant-magnitude spectral representation between f_L and f_H [21]. It should be mentioned that, in this example, the chipless tag is configured such that it preserves the polarization of the incident wave for the backscattered wave, while it is also possible to have a depolarizing configuration for the chipless tag [17]. Based on the LTI model, the frequency domain backscattering response of the chipless tag can be described as [26]

$$Y(f) = X(f) \cdot [a\,H(f)] \tag{1}$$

where $H(f)$ is related to the classical Radar Cross Section (RCS) response $[\sigma(f)]$ of the chipless tag (from the LTI model point of view, $H(f)$ is the scattering transfer function of the tag), and a represents the round trip propagation loss between the TX/RX antennas and the tag in free space. With the assumption of $f_L < f_1, f_2, f_3 < f_H$, obviously, three peaks associated with the three resonance frequencies of the dipole scatterers are observed in the tag response $Y(f)$ [Fig. 2(c)]. The basic frequency coding approach in chipless technology is to link the presence of each resonant peak in the response $Y(f)$ to the presence of each corresponding resonant scatterer on the tag. Classically, this one-to-one association is used to identify the chipless tag based on its backscattering response. Although this process is quite straightforward when the tag is placed in perfectly isolated free space, situation becomes more complex when the tag is placed in real environment. In this case, the environment can also reflect and distorts a fraction of the emitted signal. The reading process is such case is described in the next part.

2) READING PROCESS BASED ON RCS

The classical chipless reading procedure in real scenarios requires two measurements, one with the tag in the environment (Exp1) and one without the tag in the environment (Exp2). By subtracting the result of Exp2 from that of Exp1 [called background (or empty measurement) subtraction], the response of the tag can be reached. However, since the background environment mostly consists of stationary objects made of linear materials, exactly like the stationary chipless tag, it can also be modeled with an LTI system, which cause any increase in power of the transmitted signal will affect both tag and environment response with the same factor. Assume that in Exp1, the interrogating signal $X(f)$ is sent to the chipless tag when it is placed in a real environment with some stationary objects in the background [Fig. 2(a)]. The total backscattered signal can be written in frequency domain as [26]

$$Y_{tot}(f) = X(f) \cdot [a\,H(f) + E_1(f)] \tag{2}$$

where $E_1(f)$ is the transfer function of the environment seen by the TX/RX antennas and takes into account leakage, coupling and/or reflections over different objects [Fig. 2(e)]. For compensating the environment, the second measurement (Exp2) is done without the tag and can be described as

$$Y_{env}(f) = X(f) \cdot E_2(f) \tag{3}$$

where $E_2(f)$ is the transfer function of the environment without the tag [Fig. 2(d)]. Note that $E_1(f)$ and $E_2(f)$ are generally not identical due to a modification of the environment between the two measurements, and/or due to the coupling between the tag and the antenna (or any other surrounding object). By subtracting the two measurement results, the measured response of the tag is obtained as

$$Y_{mes}(f) = X(f) \cdot [a\,H(f)] + X(f) \cdot [E_1(f) - E_2(f)] \tag{4}$$

where $\epsilon(f) = E_1(f) - E_2(f)$ is defined as the transfer function of the residual environment [26] [Fig. 2(f)]. In practice, as it is shown in Fig. 2(f), the Power Spectral Density (PSD) associated to $|X(f)\,[E_1(f) - E_2(f)]|^2$ is significantly higher than the reader sensitivity (linked to the noise floor of the instrument). In addition, since both the tag and the residual environment are linear systems, increasing the transmitted energy leads to an increment in the backscattered energy from both the tag and the residual environment, while the tag-to-residual environment response ratio remains constant. This leads to the very significant result that (unlike LTV systems) as we will see in the next section, it is not possible to increase the read range by increasing the power emitted by the reader.

3) READ RANGE

The maximal reading distance of a chipless tag can be expressed as [26]

$$d_c \leq \sqrt[4]{\frac{G_t G_r \lambda^2 \sigma(f)}{(4\pi)^3 |\epsilon(f)|^2}} \tag{5}$$

where G_t and G_r are respectively the gain of the transmitting and receiving antennas. Equation (5) clearly shows how chipless read range (as an LTI transponder) is related to the RCS of the tag while it is limited due to the residual environment. To have an idea, assuming $G_t = G_r = 8$ dB and $\lambda = 0.1$ m, for a short-circuited half wavelength dipole scatterer with RCS of $\sigma = -17$ dBsm, since the typical value of the residual environment is $|\epsilon(f)|^2 = -50$ dBm, the maximum read range is obtained as 63 cm which is independent of transmitted power. Note that the read range obtained in (5) is totally different from what is calculated based on the classical radar equation as

$$d \leq \sqrt[4]{\frac{P_t G_t G_r \lambda^2 \sigma(f)}{(4\pi)^3 P_{r\,\min}}} \tag{6}$$

in which P_t is the transmitted power and $P_{r\,\min}$ is the sensitivity of the receiver. Obviously, contrary to (6), the chipless read range given in (5) does not depend on the transmitted power nor the sensitivity of the reader, and it is generally much lower than the one obtained by (6) [26]. Worth mentioning that, (6) is widely and accurately used in classical radar applications where mostly backscattering from the aircraft is not so much affected by the background environment, as the antennas almost see the free space in the sky. This fact is in contrast with what is usually going on in chipless technology where the tag should be detected in a crowded background environment.

B. MOTION-MODULATED CHIPLESS: LTV TRANSPONDER BASED ON DIFFERENTIAL RCS

1) PRINCIPLE

To differentiate the backscattering contribution of the chipless tag from that of the environment, and so to overcome the read range limitation of the chipless technology, breaking the time-invariant property of the chipless tags by utilizing the motion effect is the main idea in motion-modulated chipless RFID. Basically, this technique can be applied to identify or sense properties of any moving object while the modulation type induced by the movement depends on the motion trajectory and on how the chipless tag is reconfigured with respect to the incident wave during the motion. Generally, as it is shown in Fig. 3(a), since the position and orientation of the scatterers on the chipless tag are modified during the movement, for a time-harmonic incident wave, the backscattered wave can be modulated in terms of magnitude, phase, or polarization over the time, which results in a mixed amplitude-phase modulation on the received signal.

Fig. 3(a) shows the same frequency-coded chipless tag as introduced before while it is moving in space along the trajectory of $\vec{r}(t)$. The tag is assumed in an environment composed of stationary objects. Similar to the chipless scenario, to demonstrate the principle of operation, the moving chipless tag is considered as an LTV system whereas the environment is still modeled with an LTI system. Since the moving chipless tag (as an LTV transponder) cannot be anymore described by transfer functions, the backscattering process is formulated in time domain, and its frequency domain representation is illustrated in Fig. 3(b)–(f). Using the slow time-varying approximation [28], for a CW input signal $A_0 \cos(2\pi f_0 t)$, the output of an LTV system can be expressed by $A_0 A(t) \cos(2\pi f_0 t + \phi(t))$ where $A(t)$ and $\phi(t)$ respectively models the amplitude and phase modulation induced by the LTV system on the input CW signal. As the time-variation associated to movements are usually much smaller than the frequency of input RF carrier, the motion-induced modulation will generate frequency components close around of the carrier frequency in the spectral representation of the output. Accordingly, the interrogating signal $x(t)$ in this technique is considered as a multi-tone CW signal with stepped components between f_L and f_H as

$$x(t) = \sum_{i=1}^{N} A_0^i \cos(2\pi f_0^i t) \tag{7}$$

with the spectral representation $X(f)$ shown in Fig. 3(b). Based on the slow time-varying assumption, the response of the moving chipless tag can be written by

$$y(t) = \sum_{i=1}^{N} a(f_0^i) A_0^i A^i(t) \cos[2\pi f_0^i t + \phi^i(t)] \tag{8}$$

where $A^i(t)$ and $\phi^i(t)$ are respectively the amplitude and phase modulation induced on each CW component, and $a(f_0^i)$ is the propagation loss at each carrier frequency. Assuming that three components of $X(f)$ correspond with the three resonances of the chipless tag, the frequency-domain response of the tag $Y(f)$ can be illustrated as Fig. 3(c) in which the motion-modulated portion of the tag response is depicted by green side lobes around the three resonance-associated components (red impulses at f_1, f_2, and f_3). Also, the response of the environment as an LTI system can be written as

$$y_{env}(t) = \sum_{i=1}^{N} A_0^i |E(f_0^i)| \cos[2\pi f_0^i t + \angle E(f_0^i)] \tag{9}$$

where $E(f)$ is the transfer function of the environment. Thus, the spectrum of the environment response $Y_{env}(f)$ can be shown as Fig. 3(d), and that of the total received signal $Y_{tot}(f)$ is obtained by summing $Y(f)$ and $Y_{env}(f)$, which is presented in Fig. 3(e). As the main advantage compared to classical chipless, the motion-modulated part of the tag response will not be affected anymore by the environment response, which means the modulated part can be captured directly from the total received signal $Y_{tot}(f)$ while no background subtraction is needed.

2) READING PROCESS BASED ON DIFFERENTIAL RCS

The concept of differential RCS (or delta-RCS) has been originally introduced for chipped UHF tags based on the two load impedance which are connected to the tag antenna during the switching process [29]. However, in [30], the definition of the differential RCS has been generalized for any LTV transponder based on the spectral analysis of the modulated backscattered signal. Basically, according to [30], when an

LTV transponder is excited with a single-tone CW signal, its differential RCS is directly related to the modulated part of the backscattered power which is carried by the new frequency components (around the carrier) generated due to modulation. This modulated power is called differential backscattered power $P_{bs\,d}$, and for the motion-modulated chipless tag it can be obtained as

$$P_{bs\,d}(f_0^i) = \int_{B_i} |Y_{tot}(f)|^2\, df \tag{10}$$

where b and ϵ_m are the parameters of the carrier-excluded integration bandwidth $B_i = [f_0^i - b, f_0^i - \epsilon_m] \cup [f_0^i + \epsilon_m, f_0^i + b]$ around each carrier f_0^i which is shown in Fig. 3(e). The PSD associated to the differential backscattered power $|Y_d(f)|^2$ is shown in Fig. 3(f). The value of $P_{bs\,d}(f_0^i)$ is non-zero at the three carriers linked to the resonances of the chipless tag ($f_0^i = f_1, f_2, f_3$) and zero for the other ones, which demonstrates the motion-modulated chipless tag can be identified based on the differential backscattered power. However, since the received $P_{bs\,d}$ depends on the distance between the antennas and the tag, it is necessary to define a distance-independent quantity as differential RCS σ_d for general identification goals. Accordingly, if the distance between the TX/RX antennas and the moving tag is assumed d_m, the differential RCS of the motion-modulated chipless tag is obtained as

$$\sigma_d(f_0^i) = \frac{(4\pi)^3 (d_m)^4 P_{bs\,d}(f_0^i)}{\lambda^2 G_r G_t P_t} \tag{11}$$

at each carrier frequency, where P_t is the power of the transmitted CW components (the same for all components). Obviously, according to (10) and (11), the profile of σ_d is exactly proportional to the differential backscattered power, and consequently, the motion-modulated chipless tag can be identified based on the differential RCS. Worth mentioning that, the ID information retrieved form the differential RCS is linked to structural properties of the chipless tag (e.g. resonance frequencies here) and not to the motion characteristics, while the motion effect is just used to modulate the tag ID on the backscattered wave. Nevertheless, through the reading process, it is always possible to extract the motion characteristics (like velocity, acceleration, and period of the movement for periodic motions) or other properties of the moving object (like temperature and humidity) as a sensing application.

3) READING ROBUSTNESS AND READ RANGE

In contrast to the classical chipless, as it is shown in Fig. 3(f), the PSD of the differential backscattered power $|Y_d(f)|^2$ is not affected by the residual environment response anymore, and it is limited just by the noise floor of the reader (reader sensitivity). In other words, for example, if a CW wave is sent at f_0 frequency, for classical chipless technology, the backscattering from the tag and the environment will be both received at f_0 where the environment contribution can blind the tag response. However, for motion-modulated chipless tags, the backscattering from the tag is received at the modulated sidebands around f_0 [green side lobes in Fig. 3(e)] while the environment response is still located at f_0 [purple impulses in Fig. 3(e)] and it does not affect the tag response. This fact demonstrates that the reading process for motion-modulated chipless tags is much more robust against the environment clutter. However, of course, as the reading distance increases for motion-modulated tags, the multipath effect (multi-reflection of the modulated tag response from objects in the environment) can degrade the performance of the reading process like what is always raised in telecommunication.

The maximal read range of the motion-modulated chipless tag is achieved based on the classical radar [(6)], while it should be modified with the differential RCS (σ_d) instead of RCS (σ) as [26]

$$d_m \leq \sqrt[4]{\frac{P_t G_t G_r \lambda^2 \sigma_d(f)}{(4\pi)^3 P_{r\ \min}}} \tag{12}$$

which clearly shows that the maximum read range of the motion-modulated chipless tags is not limited and it can be increased by increasing the transmitted power, using readers with lower sensitivity, and designing motion-modulated chipless tags with higher differential RCS, although the latter is mostly dependent on the motion trajectory and its characteristics.

4) MODULATION SCHEME

The modulation type induced by the motion and also its modulation index (or modulation depth) [31] (which describes how much the modulated variable of the carrier signal (amplitude or phase) varies around its unmodulated level) depends on how the backscattered wave is modified by the moving chipless tag in terms of phase, polarization, and magnitude. Nevertheless, specific scatterers (and so chipless tags) with designed motion trajectories can be proposed to only modulate the backscattered wave with phase (or Doppler), polarization, or magnitude, which leads to a pure amplitude or phase modulation on the received signal. This approach will be helpful to precisely characterize the tag ID and possibly to sense the motion properties or the moving object characteristics. In the following sections, we present different types of the motion-modulated chipless tag which have been employed to implement different modulation types which can be used for identification and sensing applications.

III. DOPPLER-MODULATED CHIPLESS TAGS

A. ROTATIONAL MOTION

1) DESCRIPTION

Fig. 4 presents the Doppler-modulated chipless tag based on the rotational motion [32]. To just modulate the backscattered wave in phase (Doppler effect) during the rotation, the short-circuited dipole scatterer is rotated such that it is aligned with the incident wave polarization (aligned along z-axis with the z-polarized incident plane wave). As it shown in Fig. 4, in this configuration, the magnitude and polarization of the backscattered wave will not be modified during the

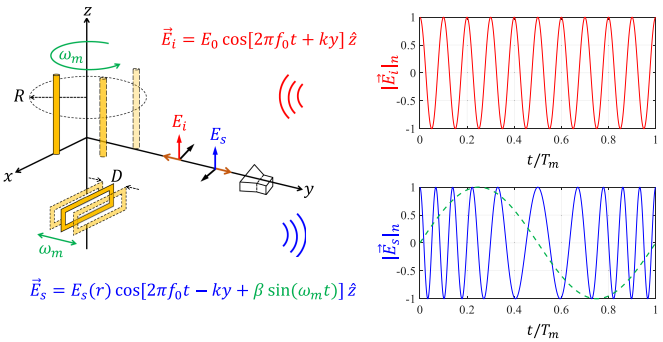

FIGURE 4. Phase (Doppler)-modulated chipless tag. The normalized magnitude of the incident and scattered field is shown as a function of time during one period of motion ($T_m = 2\pi/\omega_m$) respectively in red and blue color. The phase modulating waveform induced by the motion is also shown for better interpretation with dashed green line.

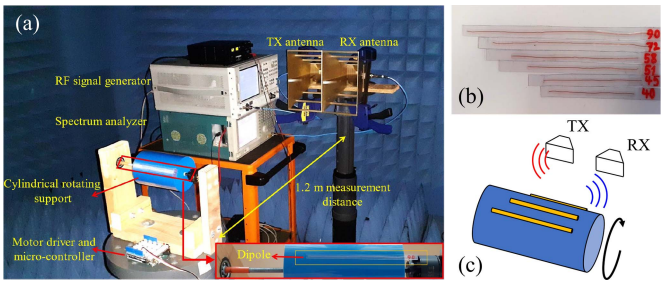

FIGURE 5. (a) Measurement bench used for identification of the rotating Doppler-modulated chipless tag. (b) Chipless tag consists of dipole scatterers. (c) Configuration of the dipoles on the rotating cylindrical support [32].

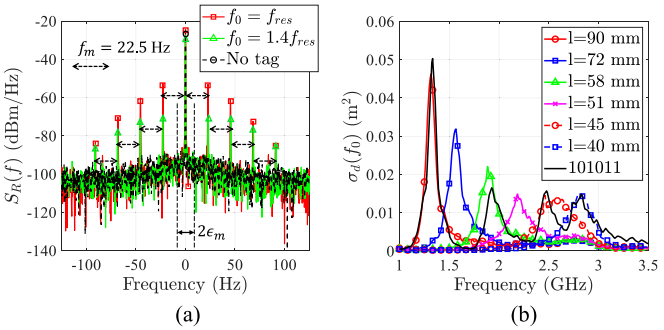

FIGURE 6. (a) Measured PSD of the backscattered signal from rotating Doppler-modulated chipless tag. (b) Measured differential RCS of the Doppler-modulated chipless tag [32].

rotation, while just its phase is modulated proportional to the rotational movement. The Doppler modulation induced by the rotation (as a periodic motion), is observed as a sinusoidal time-varying phase (shown by green color in Fig. 4) $\beta \sin(\omega_m t)$ where $\beta = 4\pi R/\lambda$ is the modulation index in which R is the radius of rotation, and $\omega_m = 2\pi f_m$ is the angular frequency of the motion. The sinusoidal phase variation in time-domain, will be translated to frequency components at nf_m $n = 0, \pm1, \pm2, \ldots$ around the carrier f_0 with the respective amplitudes of $J_n(\beta)$, where $J_n(x)$ is the Bessel function of the first kind of order n. Using the unitary property of the Bessel harmonics $\left(\sum_{n=-\infty}^{+\infty} |J_n(x)|^2 = 1\right)$, the analytic expression of the differential RCS for the rotating dipole scatterer can be obtained as [32]

$$\sigma_d(f_0) = \sigma(f_0)[1 - J_0^2(\beta)] \tag{13}$$

which is directly related to the RCS of the dipole $\sigma(f_0)$ with the factor of $[1 - J_0^2(\beta)]$. Equation (13) shows that the maximum achievable differential RCS is equal to the RCS of the dipole, and it can be reached if the rotation radius R is optimally selected such that, at the resonance frequency, $J_0(\beta) = 0$.

2) MEASUREMENT

The measurement bench used to verify the rotational Doppler-modulated chipless tag is shown in Fig. 5(a) composed of an RF signal generator (HP 8720D) and a spectrum analyzer (Tektronix RSA3408 A) that are respectively connected to the closely placed TX and RX antennas (monostatic configuration) [A.H. Systems SAS-571], while both instruments are synchronized using a 10-MHz reference signal. The transmission frequency (f_0) can be set in-between 1 and 3.5 GHz with the desired step and the output power (P_t) has been set to 0 dBm [32]. The chipless tag is implemented by six different-length dipole scatterers shown in Fig. 5(b) resonating at 1–3.5 GHz ($f_L = 1$ and $f_H = 3.5$ GHz) bandwidth. The rotation is realized using a motor-driven cylindrical support with the optimum radius of $R = 35$ mm on which chipless tags are attached as shown in Fig. 5(c). The measured PSD of the backscattered wave from a single rotating dipole is illustrated in Fig. 6(a) at two different carriers while one of them exactly correspond to the resonance of the dipole ($f_0 = f_{res}$) and the other is at $f_0 = 1.4 f_{res}$. In addition to the clearly observable rotation induced frequency components at $n \times 22.5$ Hz [associated with Bessel harmonics $J_n(\beta)$] around the carrier in both cases, the large difference between the amplitude of the modulated components in two cases ($\approx$20 dB) demonstrates how the resonance of the dipole can be effectively detected based on the differential backscattered power, and consequently differential RCS, at large distances (1.2 m in this example). Moreover, note that when the dipole is not attached to the rotating support, there is no modulated harmonics around the carrier, which means the σ_d of the environment will be much smaller than that of the rotating chipless tag [32].

3) IDENTIFICATION

By sending a sequence of CW carriers between 1 and 3.5 GHz (f_0^i $i = 1, 2, \ldots$), the measured differential RCS associated with each single-dipole tag and also that of a multi-dipole tag (composed of four dipoles) are calculated based on (10) and (11) which is shown in Fig. 6(b). Obvious resonance peaks linked to each dipole scatterer prove the identification process based on the differential RCS for rotational Doppler-modulated chipless tags [32].

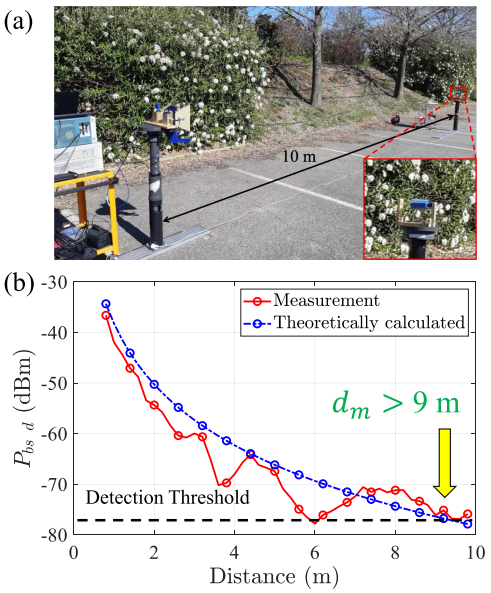

FIGURE 7. (a) Read range measurement in a real environment. (b) Differential backscattered power as a function of distance [32].

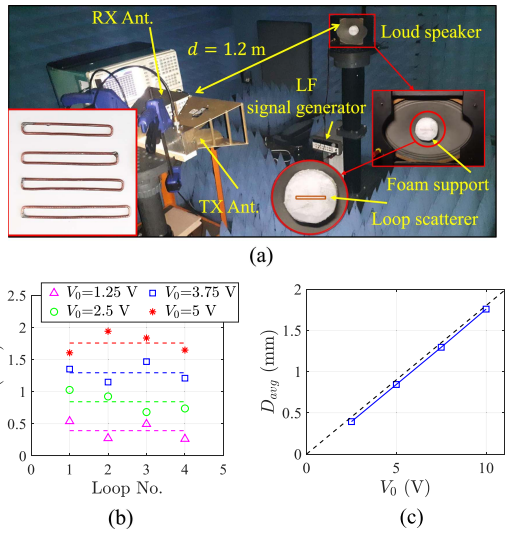

FIGURE 8. (a) Measurement bench used for vibration sensing using Doppler-modulated chipless tag. Chipless tag composed of rectangular loop scatterers is shown in the inset. (b) Detected vibration amplitude by use of Doppler-modulated chipless tag. (c) Averaged detected vibration amplitude [33].

4) READ RANGE

The maximal read range of the Doppler-modulated chipless tag can be estimated using (12) with the calculated differential RCS shown in Fig. 6(b). To experimentally verify the results obtained from (12), the maximum achievable read range of the rotating tag (90 mm length dipole) is measured in a real environment as it is shown in Fig. 7(a). The measured $P_{bs\,d}$ is plotted as a function of distance in Fig. 7(b) which is in good agreement with the results theoretically obtained based on (12). According to the sensitivity of the used reader (spectrum analyzer), the detection threshold of the tag is measured at $P_{r\,\min} = -78$ dBm which leads to the maximum read range of almost 10 m with $P_t = 5$ dBm. The achieved maximum read range for the Doppler-modulated chipless tag outperforms the classical chipless read range by at least a factor of 10, which is a great improvement in terms of reading distance as it was expected [32].

B. VIBRATIONAL MOTION

1) DESCRIPTION

The other Doppler-modulated chipless tag realized based on vibration is shown in Fig. 4 [33]. The chipless tag is considered with a rectangular loop scatterer which is aligned such that the backscattered wave (generated by the fundamental mode of the loop) preserves the same polarization as the incident wave (z-aligned). The loop has a one-dimensional vibration along the direction of the incident wave (y-axis) which induces a sinusoidal phase modulation on the backscattered wave same as the rotational case, while the modulation index for the vibration case is defined as $\beta = 2\pi D/\lambda$ where D is the vibration amplitude. Since the modulation scheme is the same for the rotating dipole and the vibrating loop, the differential RCS of the vibrating loop is also expressed by (13) [33]. The performance of the vibrational Doppler-modulated chipless tag in terms of identification and read range is almost similar to the rotational case [33] which is not presented here to avoid redundancy. However, it should be mentioned that the β value in practical vibrations is usually quite small (due to the small vibration amplitude respect to the wavelength) which cause to reduce the differential RCS level significantly [see (13)]. Nevertheless, it is demonstrated in [33] that resonant scatterers such as a rectangular loop can be utilized to sense the vibration characteristics (amplitude and frequency) more efficiently and at larger distances compared to when chipless tags are not attached to the vibrating surface. Accordingly, the measurement results related to the vibration sensing using Doppler-modulated chipless tag is presented in the next part.

2) VIBRATION SENSING

The measurement setup for vibration sensing is shown in Fig. 8(a) [33]. The vibration is produced using a loud speaker which is fed by a LF signal generator with the sinusoidal voltage of $V_0 \sin(2\pi f_m t)$ where $f_m = 68$ Hz. Four rectangular loop scatterers used for the sensing are also shown in the inset of Fig. 8(a). The loops are attached to the speaker with a foam support. By measuring the PSD of the backscattered wave at the resonance frequency of each loop, and using a least-square estimator based on successive Bessel harmonics ratios [33], the vibration amplitude is detected at four different levels of the speaker feed voltage $V_0 = 1.25,\ 2.5,\ 3.75,\ 5$ V. The corresponding estimated vibration amplitudes are presented in Fig. 8(b) for the four loops which are compatible with each other demonstrating the validity of the vibration sensing performance. Moreover, the average estimated vibration amplitudes is presented in Fig. 8(c) as a function of V_0 which perfectly follows the linear variation of the small signal

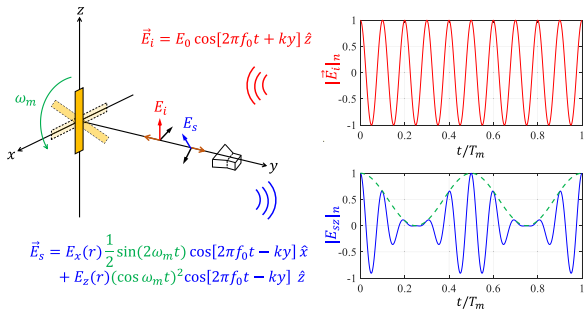

FIGURE 9. Polarization-modulated chipless tag. The normalized magnitude of the incident and scattered field is shown as a function of time during one period of motion ($T_m = 2\pi/\omega_m$) respectively in red and blue color. The amplitude modulating waveform induced by the motion is also shown for better interpretation with dashed green line.

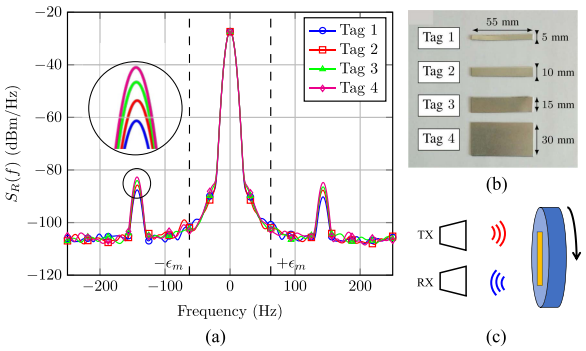

FIGURE 10. (a) Measured PSD of the backscattered signal from polarization-modulated chipless tags. Identification is realized based on the amplitude of the side lobes. (b) Chipless tag formed by strip dipole scatterers. (c) Configuration of the tags on the rotating circular support [34].

approximation [33]. This example shows that it is possible to measure vibration amplitudes well below one millimetre with a very good accuracy while working with a carrier frequency of a few GHz.

IV. POLARIZATION-MODULATED CHIPLESS TAGS

A. DESCRIPTION

The polarization-modulated chipless tag is presented in Fig. 9. The chipless tag is a strip dipole located at xz-plane which is rotated around y-axis such that it center point coincide with the origin. The incident plane wave impinges normally on the rotating strip dipole with a vertical polarization (z-polarized) [34]. Since the orientation of the tag is varying during the rotation, the two polarization components of the backscattered wave will be modulated by the tag. Suppose that, at the initial moment when the dipole is aligned with z-axis, the backscattered wave is expressed using the polarimetric scattering matrix $[S]$ as

$$\begin{bmatrix} E_s^v \\ E_s^h \end{bmatrix} = \begin{bmatrix} S_{vv} & S_{vh} \\ S_{hv} & S_{hh} \end{bmatrix} \begin{bmatrix} E_i^v \\ E_i^h \end{bmatrix} \tag{14}$$

where v and h polarization respectively corresponds to z and x polarization in Fig. 9. For the described scattering configuration, it is shown that the backscattered wave during the rotation can be written as [34]

$$[E_s] = [\Omega(\theta)]^T \cdot [S] \cdot [\Omega(\theta)] \cdot [E_i] \tag{15}$$

where $\Omega(\theta)$ is the rotation matrix associated with the time-varying rotation angle of $\theta(t) = \omega_m t$. Using (14), the expression of the two polarization components of the backscattered wave is obtained as it is indicated in Fig. 9, while the modulation is done on the amplitude of the two field components with two trigonometric functions of time (marked in green color in Fig. 9). Note that the phase of the backscattered wave is not modified by the rotating tag due to the symmetry of the scatterer. Obviously, for example, if the backscattered wave is captured by the antenna with the same polarization as incident wave (vertical polarization), the polarization modulation induced by the chipless tag is observed as an amplitude modulation on the received signal as it is shown in Fig. 9. The amplitude modulation in time-domain produce two frequency components at $\pm 2f_m$ around the carrier frequency f_0 in the spectral domain. Accordingly, the differential RCS of the polarization-modulated chipless tag can be obtained in terms of polarimetric scattering parameters as [35]

$$\sigma_d(f_0) = 4\pi \frac{|S_{vv}(f_0) - S_{hh}(f_0)|^2 + 4|S_{vh}(f_0)|^2}{8} \tag{16}$$

which is quite similar to (13) as it relates the σ_d to the static scattering parameters. However, in contrast to (13) obtained for Doppler-modulated chipless tags, the differential RCS of the polarization-modulated tag (16) does not depend on the motion characteristics (like the rotation radius or vibration amplitude in case of Doppler-modulated tags) and it is just determined based on the polarimetric scattering characteristic of the used scatterer in the chipless tag which is linked to geometrical properties of the scatterer [34].

B. RESULTS

1) IDENTIFICATION

Using the same measurement bench as Fig. 5(a) (both TX and RX antennas in vertical polarization), the PSD of the backscattered wave from polarization-modulated chipless tags are captured as shown in Fig. 10(a) [34]. Four chipless tags formed by aluminium-made strip dipoles are used in measurements, which are presented in Fig. 10(b). The transmitted carrier is set at $f_0 = 915$ MHz with $P_t = 0$ dBm. Similar to Fig. 5(a), the tags are attached to a circular support like what is shown Fig. 10(c), and it is rotated using a motor with rotational frequency of $f_m = 71$ Hz. The tag ID in this case is associated to the magnitude of the differential backscattered power (instead of resonance frequencies in spectral behaviour of the $P_{bs\,d}$ for the Doppler-modulated tags). Accordingly, the amplitude of the two modulation-induced frequency components at $\pm 2f_m = \pm 142$ Hz is investigated to identify the four designed chipless tags. Obviously, as it is shown in Fig. 10(a), the highest level of the modulated component is associated with the biggest tag (Tag 4), and the lower ones are consecutively associated with Tag 3, Tag 2, and Tag 1 [34].

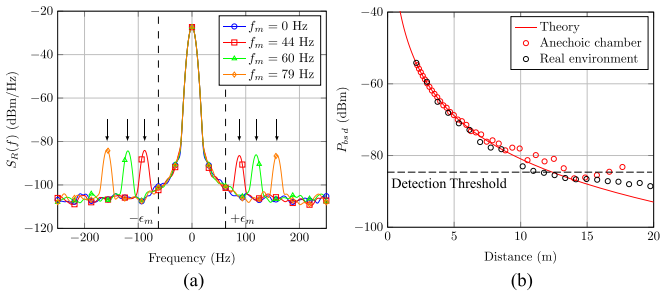

FIGURE 11. (a) Measured PSD of the backscattered signal from polarization-modulated chipless tag for different rotational speed. Sensing is realized based on the frequency position of the side lobes. (b) Differential backscattered power as a function of distance [34].

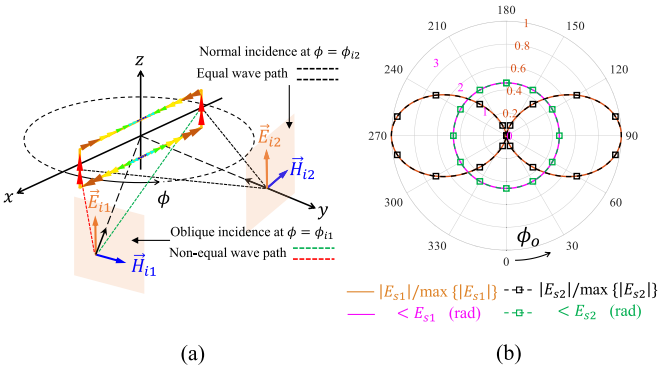

FIGURE 12. (a) Symmetric resonant rectangular loop scatterer proposed for Doppler suppression. (b) The azimuth distribution of the phase and normalized magnitude of the scattered electric field for two incidence angles (normal and oblique) [36].

2) SENSING

As a sensing application, the rotational speed of the tag can be also detected based on the modulation-induced frequency components observed in the captured PSD. Note that as these components appear at $\pm 2f_m$, the rotational frequency is half of the frequency of the measured components. Fig. 11(a) illustrates the rotational speed sensing capability using polarization-modulated chipless tags. As it is shown, the tag is rotated at different speeds, and the rotational frequency can be retrieved easily from the location of the modulation-induced components [34].

3) READ RANGE

Finally, the maximum achievable reading distance of the polarization-modulated chipless tag is examined experimentally with results presented in Fig. 11(b). The differential backscattered power from rotating Tag 4 is measured in an anechoic chamber and in a real environment, and the measured results are compared with what can be calculated based on (11). As it can be observed the results are in good agreement, and the polarization-modulated tag can be read at distances up to 13 m with $P_t = 36$ dBm and $f_0 = 915$ MHz [34].

V. DIRECTION-MODULATED CHIPLESS TAGS

A. PRINCIPLE

The last type of motion-modulated chipless tags is proposed as direction-modulated tags [36]. Following the two previous types [phase (Doppler) and polarization modulated tags], this type of tags should modulate the backscattered wave just in magnitude (and not in phase or polarization) during the motion. Although it is not difficult to find moving scatterers that do not depolarize the reflected wave (like rotating dipoles in Section III or any other structure which can be perfectly aligned with the incident field), a moving structure that does not modulate the backscattered phase (while it has a radial velocity toward the incident direction) can not be realized easily. However, since usually the scatterers (when they are impinged by EM wave) have a specific reradiation pattern (or RCS pattern) in space which can be strong in one "direction" and weak in the other "direction", the rotation of the scatterer in space can modify the backscattered wave just in magnitude, provided that the phase (Doppler) modulation induced by rotation is suppressed somehow. Fig. 12(a) shows a rectangular loop scatterer centered at the origin and aligned with z-axis. Assume that the loop is impinged by a z-polarized wave from two directions: the first one, a general oblique incidence at $\phi = \phi_{i1}$ and the second one, a normal incidence at $\phi = \phi_{i2} = \pi/2$. Also assume that the carrier frequency is chosen such that the fundamental resonant mode of the loop scatterer is excited with the mode current shown in Fig. 12(a). At the azimuth plane (xy-plane), the reflected wave for all incidence angles ($\phi = \phi_{i1}$ and ϕ_{i2}) has the same vertical polarization (z-polarization) as the incident wave. In addition, using a full-wave simulation, the azimuth distribution of the phase and normalized magnitude of the scattered electric field can be obtained as shown in Fig. 12(b) for both incidence angles. The key point is that, for both cases, which means for all the incidence angles in the azimuth plane, the backscattered field has the same phase and magnitude distribution. Moreover, the azimuth phase distribution is perfectly uniform for all incidence angles. In other words, this specific scatterer can modify the magnitude of the backscattered wave proportional to its reradiation pattern when it is rotated around its symmetry axis (z-axis), while the phase and polarization of the backscattered wave are not modified at all. Note that during the rotation, different points of the loop have a non-zero radial velocity towards the incidence direction, however, the phase of the induced current is not modulated due to the resonance effect, which means the Doppler effect is suppressed by the resonance of the scatterer [36].

B. DESCRIPTION

Fig. 13 presents the direction-modulated chipless tag which is designed based on the proposed principle. The resonant rectangular loop is rotating around its symmetry axis z-axis and it is impinged by a z-polarized wave. Accordingly, the magnitude of the backscattered field is modulated proportional to the reradiation pattern of the loop at its fundamental

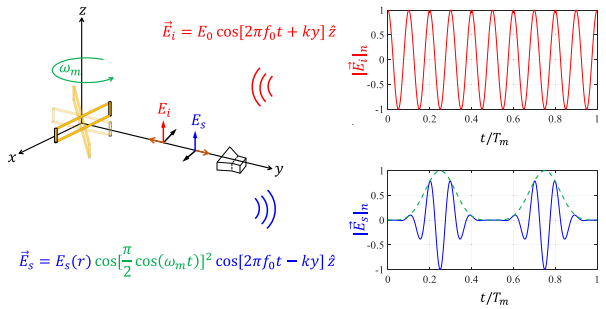

FIGURE 13. Direction-modulated chipless tag. The normalized magnitude of the incident and scattered field is shown as a function of time during one period of motion ($T_m = 2\pi/\omega_m$) respectively in red and blue color. The amplitude modulating waveform induced by the motion is also shown for better interpretation with dashed green line.

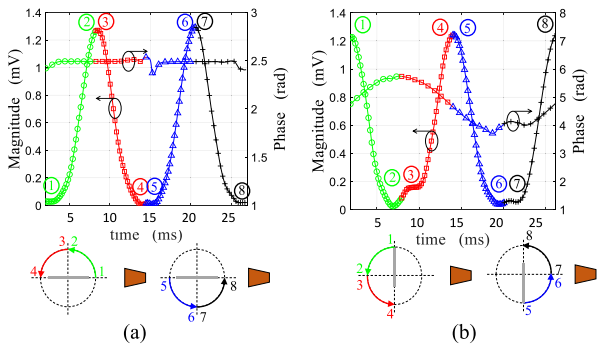

FIGURE 14. The magnitude and phase variation of the measured backscattered signal from (a) symmetrically (b) non-symmetrically rotating loop during one period of rotation. The respective orientation of the loop at each quarter of the rotation cycle is linked with the waveform by colors and numbers to illustrate the directional amplitude modulation [36].

mode, whereas the phase and polarization of the reflected wave are not affected by the rotating loop. According to the azimuth reradiation pattern of the loop $\cos(\pi/2\cos(\phi))$, the magnitude of the backscattered field is modulated in time as it is indicated by the green color function in Fig. 13. Obviously, this directional modulation is observed as a pure amplitude modulation on the received signal as it is shown in Fig. 13 [36].

C. RESULTS

The concept is verified experimentally using the same bench as Fig. 5(a), while the loop is rotated by the motor with two configurations as symmetrical and non-symmetrical rotation, which are respectively shown in Fig. 14(a) and (b). The phase and amplitude of the received signal in both configurations are plotted in Fig. 14(a) and (b) as a function of time (during one period of rotation). As it can be observed, the amplitude of the received signal in both configurations varies proportionally to the reradiation pattern of the loop at each rotation cycle. To clarify that, in Fig. 14(a) and (b), each rotation cycle is divided into four quarters (depicted in green, red, blue, and black color) and the link between the orientation of the loop and its corresponding amplitude signal state is shown by colors and numbers. This illustration proves the directional amplitude modulation induced by the rotating loop in both configurations. However, the phase of the received signal is constant over the time only for the symmetric configuration and it is sinusoidally varying for the non-symmetric case, which demonstrates that a pure directional amplitude modulation can be achieved only when both the symmetry property and the Doppler suppression due to resonance is utilized simultaneously [36].

VI. CONCLUSION AND FUTURE OUTLOOK

The concept of motion-modulated chipless RFID was established in this paper. The feasibility of the idea in terms of read range enhancement was proven theoretically and verified in the experiment, where the reading distance of more than several meters was achieved for motion-modulated chipless tags. Different types of motion-induced modulation were considered analytically to obtain the expression for associated differential RCS. Although the concept was addressed for some familiar periodic motions like rotation and vibration, the principle holds for any motion trajectory. Accordingly, in the future, the idea can be applied in more practical cases like tagged objects carried by a conveyor belt or human hands holding a tag. Moreover, the presented precise analysis for modulation schemes and their resultant signal expressions can be exploited in some sensing and localization scenarios.

REFERENCES

[1] P. V. Nikitin and K. Rao, "Harmonic scattering from passive UHF RFID tags," in *Proc. IEEE Antennas Propag. Soc. Int. Symp.*, 2009, pp. 1–4.
[2] D. Mascanzoni and H. Wallin, "The harmonic radar: A new method of tracing insects in the field," *Ecological Entomol.*, vol. 11, no. 4, pp. 387–390, 1986.
[3] A. G. Bell, "The photophone," *Science*, no. 11, pp. 130–134, 1880.
[4] P. Nikitin, "Leon Theremin (Lev Termen)," *IEEE Antennas Propag. Mag.*, vol. 54, no. 5, pp. 252–257, Oct. 2012.
[5] H. Stockman, "Communication by means of reflected power," *Proc. IRE*, vol. 36, no. 10, pp. 1196–1204, 1948.
[6] L. Bowden, "The story of IFF (identification friend or foe)," *IEE Proc. A*, vol. 132, no. 6, pp. 435–437, 1985.
[7] K. Finkenzeller, *RFID Handbook*. Hoboken, NJ, USA: Wiley, 2010.
[8] R. Want, "An introduction to RFID technology," *IEEE Pervasive Comput.*, vol. 5, no. 1, pp. 25–33, Jan.–Mar. 2006.
[9] D. Paret, *RFID at Ultra and Super High Frequencies: Theory and Application*. Hoboken, NJ, USA: Wiley, 2009.
[10] E. Perret, *Radio Frequency Identification and Sensors: From RFID to Chipless RFID*. Hoboken, NJ, USA: Wiley, 2014.
[11] R. Rezaiesarlak and M. Manteghi, *RFID Chipless*. Berlin, Germany: Springer, 2016.
[12] S. Preradovic and N. C. Karmakar, "Chipless RFID: Bar code of the future," *IEEE Microw. Mag.*, vol. 11, no. 7, pp. 87–97, Dec. 2010.
[13] A. Vena, E. Perret, and S. Tedjini, "Chipless RFID tag using hybrid coding technique," *IEEE Trans. Microw. Theory Techn.*, vol. 59, no. 12, pp. 3356–3364, Dec. 2011.
[14] F. Costa, S. Genovesi, and A. Monorchio, "A chipless RFID based on multiresonant high-impedance surfaces," *IEEE Trans. Microw. Theory Techn.*, vol. 61, no. 1, pp. 146–153, Jan. 2013.
[15] A. Vena, E. Perret, and S. Tedjini, "High-capacity chipless RFID tag insensitive to the polarization," *IEEE Trans. Antennas Propag.*, vol. 60, no. 10, pp. 4509–4515, Oct. 2012.
[16] M. Khaliel, A. El-Awamry, A. Fawky Megahed, and T. Kaiser, "A novel design approach for co/cross-polarizing chipless RFID tags of high coding capacity," *IEEE J. Radio Freq. Identification*, vol. 1, no. 2, pp. 135–143, Jun. 2017.

[17] A. Vena, E. Perret, and S. Tedjni, "A depolarizing chipless RFID tag for robust detection and its FCC compliant UWB reading system," *IEEE Trans. Microw. Theory Techn.*, vol. 61, no. 8, pp. 2982–2994, Aug. 2013.
[18] F. Costa et al., "A depolarizing chipless RF label for dielectric permittivity sensing," *IEEE Microw. Wireless Compon. Lett.*, vol. 28, no. 5, pp. 371–373, May 2018.
[19] F. Babaeian and N. C. Karmakar, "Development of cross-polar orientation-insensitive chipless RFID tags," *IEEE Trans. Antennas Propag.*, vol. 68, no. 7, pp. 5159–5170, Jul. 2020.
[20] A. Ramos, E. Perret, O. Rance, S. Tedjini, A. Lázaro, and D. Girbau, "Temporal separation detection for chipless depolarizing frequency-coded RFID," *IEEE Trans. Microw. Theory Techn.*, vol. 64, no. 7, pp. 2326–2337, Jul. 2016.
[21] N. C. Karmakar et al., *Chipless RFID Reader Architecture*. Norwood, MA, USA: Artech House, 2013.
[22] M. Garbati, R. Siragusa, E. Perret, A. Vena, and C. Halopé, "High performance chipless RFID reader based on IR-UWB technology," in *Proc. IEEE 9th Eur. Conf. Antennas Propag.*, 2015, pp. 1–5.
[23] F. Costa et al., "Robust reading approach for moving chipless RFID tags by using ISAR processing," *IEEE Trans. Microw. Theory Techn.*, vol. 66, no. 5, pp. 2442–2451, May 2017.
[24] M. A. Islam and N. C. Karmakar, "An 8 × 8 mm-wave LP ACMPA array for a long-range mm-wave chipless RFID tag-sensor reader," *IEEE J. Radio Freq. Identification*, vol. 5, no. 1, pp. 53–63, Mar. 2021.
[25] M. Khaliel, A. El-Awamry, A. Fawky, and T. Kaiser, "Long reading range chipless RFID system based on reflectarray antennas," in *Proc. 11th Eur. Conf. Antennas Propag.*, Paris, France, 2017, pp. 3384–3388.
[26] N. Barbot, O. Rance, and E. Perret, "Classical RFID versus chipless RFID read range: Is linearity a friend or a foe?," *IEEE Trans. Microw. Theory Techn.*, vol. 69, no. 9, pp. 4199–4208, Sep. 2021.
[27] M. S. Reynolds, "A 500°C tolerant ultra-high temperature 2.4 GHz 32 bit chipless RFID tag with a mechanical BPSK modulator," in *Proc. IEEE Int. Conf. RFID*, 2017, pp. 144–148.
[28] R. Bracewell and R. Bracewell, *The Fourier Transform and its Applications* (Electrical Engineering Series). New York, NY, USA: McGraw Hill, 2000.
[29] P. Nikitin, K. Rao, and R. Martinez, "Differential RCS of RFID tag," *Electron. Lett.*, vol. 43, pp. 431–432, Feb. 2007.
[30] N. Barbot, O. Rance, and E. Perret, "Differential RCS of modulated tag," *IEEE Trans. Antennas Propag.*, vol. 2, no. 9, pp. 10–15, Sep. 2021.
[31] A. Carlson, P. Crilly, and J. Rutledge, *Communication Systems*. New York, NY, USA: McGraw-Hill, 2002.
[32] A. Azarfar, N. Barbot, and E. Perret, "Chipless RFID based on micro-doppler effect," *IEEE Trans. Microw. Theory Techn.*, vol. 70, no. 1, pp. 766–778, Jan. 2022.
[33] A. Azarfar, N. Barbot, and E. Perret, "Vibration sensing using doppler-modulated chipless RFID tags," in *Proc. IEEE MTT-S Int. Microw. Symp.*, 2022, pp. 129–132.
[34] N. Barbot and E. Perret, "Linear time-variant chipless RFID sensor," *IEEE J. Radio Freq. Identification*, vol. 6, pp. 104–111, 2021.
[35] N. Barbot, "Delta RCS expression of linear time-variant transponders based on polarization modulation," in *Proc. IEEE 12th Int. Conf. RFID Technol. Appl.*, 2022, pp. 55–58.
[36] A. Azarfar, N. Barbot, and E. Perret, "Directional amplitude backscatter modulation with suppressed Doppler based on rotating resonant loop," *Sci. Rep.*, to be published.

ASHKAN AZARFAR (Graduate Student Member, IEEE) received the B.Sc. degree in electrical engineering from Iran University of Science and Technology, Tehran, Iran in 2014, and the M.Sc. degree in electrical engineering from the University of Tehran, Tehran, Iran in 2017. He is currently working toward the Ph.D. degree with the University of Grenoble Alpes, Grenoble INP, France. His research interests include motion-modulated chipless transponders, electromagnetic wave scattering, antenna design and wave propagation, and microwave circuits design.

NICOLAS BARBOT (Member, IEEE) received the M.Sc. and Ph.D. degrees from the University de Limoges, France, in 2010 and 2013, respectively. His Ph.D. degree work with Xlim Laboratory, Limoges, France, was focused on error-correcting codes for the optical wireless channel. He also realized a postdoctoral work in joint source-channel decoding with L2S Laboratory, Gif-sur-Yvette, France. Since September 2014, he has been an Assistant Professor with the Université Grenoble Alpes - Grenoble Institute of Technology, Valence, France. His scientific background with LCIS Laboratory, Valence, France, covers wireless communications systems based on backscattering principle which include classical RFID and chipless RFID. His research interests include transponders which can not be described by linear time-invariant systems. This gathers harmonic transponders which are based on the use of a non-linear component (Schottky diode) or linear time-variant transponders which are based on the modification of their response in the time domain. He also places special interests on antenna design and instrumentation based on these phenomenons.

ETIENNE PERRET (Senior Member, IEEE) received the Eng.Dipl. degree in electrical engineering from the Ecole Nationale Supérieure d'Electronique, d'Electrotechnique, d'Informatique, d'Hydraulique, et des Télécommunications, Toulouse, France, 2002, and the M.Sc. and Ph.D. degrees in electrical engineering from the Toulouse Institute of Technology, Toulouse, France, in 2002 and 2005, respectively. From 2005 to 2006, he held a postdoctoral position with the Institute of Fundamental Electronics, Orsay, France. He was appointed Associate Professor in 2006 and Full Professor in 2022 of electrical engineering with the University of Grenoble Alpes, Grenoble INP, France, where he heads the ORSYS Research Group (20 researchers) from 2015 to 2022. From 2014 to 2019, he was a Junior Member with the Institut Universitaire de France, Paris, France, an institution that distinguishes professors for their research excellence, as evidenced by their international recognition. From 2015 to 2020, he was an appointed Member of the French National Council of Universities. He has authored or co-authored more than 200 technical conferences, letters and journal papers, and books and book chapters and holds several patents. His works have generated more than 4200 citations. His research interests include wireless communication systems based on the principle of backscatter modulation or backscattering of EM waves especially in the field of RFID and chipless RFID for identification and sensors, electromagnetic modeling of passive devices for millimeter and submillimeter-wave applications, and advanced computer-aided design techniques based on the development of an automated codesign synthesis computational approach. Dr. Perret was a Technical Program Committee Member of the IEEE International Conference on RFID, the IEEE RFID TA, and is a member of the IMS Technical Paper Review Committee. He was the recipient of several awards such as the *MIT Technology Review*'s French Innovator's under 35 in 2013, French Innovative Techniques for the Environment Award in 2013, SEE/IEEE Leon Brillouin Award for his outstanding achievement in the identification of an object in an unknown environment using a chipless label or tag in 2016, IEEE MTT-S 2019 Outstanding Young Engineer Award, Prix Espoir IMT - Académie des sciences in 2020, and the Grand Prix de l'Electronique Général Ferrié in 2021. He was a Keynote Speaker and the Chairman of several international symposiums, and also ERC Consolidator Grant in 2017 for his Project ScattererID.